BIOCHEMISTRY
including biophysical chemistry & molecular biology

Article

pubs.acs.org/biochemistry

Increased Redox-Sensitive Green Fluorescent Protein Reduction Potential in the Endoplasmic Reticulum following Glutathione-Mediated Dimerization

Deboleena Dipak Sarkar,[†] Sarah K. Edwards,[†] Justin A. Mauser,[†] Allen M. Suarez,[†] Maxwell A. Serowoky,[†] Natalie L. Hudok,[†] Phylicia L. Hudok,[†] Martha Nuñez,[†] Craig S. Weber,[‡] Ronald M. Lynch,[‡] Osamu Miyashita,[†] and Tsu-Shuen Tsao*,[†]

[†]Department of Chemistry and Biochemistry, University of Arizona, Tucson, Arizona 85721, United States

[‡]Department of Physiology, University of Arizona Health Sciences Center, Tucson, Arizona 85724, United States

Supporting Information

ABSTRACT: As the endoplasmic reticulum (ER) is the compartment where disulfide bridges in secreted and cell surface proteins are formed, the disturbance of its redox state has profound consequences, yet regulation of ER redox potential remains poorly understood. To monitor the ER redox state in live cells, several fluorescence-based sensors have been developed. However, these sensors have yielded results that are inconsistent with each other and with earlier non-fluorescence-based studies. One particular green fluorescent protein (GFP)-based redox sensor, roGFP1-iL, could detect oxidizing changes in the ER despite having a reduction potential significantly lower than that previously reported for the ER. We have confirmed these observations and determined the mechanisms by which roGFP1-iL detects oxidizing changes. First, glutathione mediates the formation of disulfide-bonded roGFP1-iL dimers with an intermediate excitation fluorescence spectrum resembling a mixture of oxidized and reduced monomers. Second, glutathione facilitates dimerization of roGFP1-iL, which shifted the equilibrium from oxidized monomers to dimers, thereby increasing the molecule's reduction potential compared with that of a dithiol redox buffer. We conclude that the glutathione redox couple in the ER significantly increased the reduction potential of roGFP1-iL *in vivo* by facilitating its dimerization while preserving its ratiometric nature, which makes it suitable for monitoring oxidizing and reducing changes in the ER with a high degree of reliability in real time. The ability of roGFP1-iL to detect both oxidizing and reducing changes in ER and its dynamic response in glutathione redox buffer between approximately −190 and −130 mV *in vitro* suggests a range of ER redox potentials consistent with those determined by earlier approaches that did not involve fluorescent sensors.

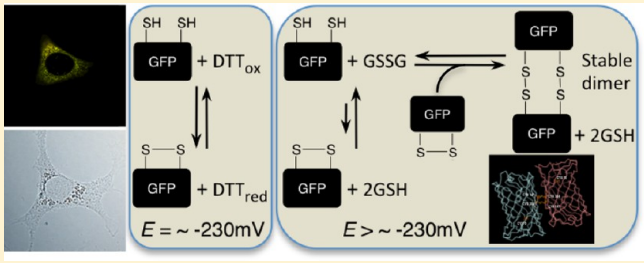

Disulfide bonding helps to stabilize protein structure[1,2] and promotes correct pairing of cysteines in proper temporal sequence, which is important for oxidative protein folding.[3,4] Failure to form the appropriate disulfide bonds may affect a protein's function and lead to a diseased state.[5−8] A redox environment conducive to the formation of disulfide bonds is critical for the oxidative folding of secreted or cell surface proteins in the endoplasmic reticulum (ER).[4,9] The ER redox environment is likely under tight regulation given the multitude of thiol oxidoreductases and low-molecular weight redox-active electron carriers that are known to play key roles in oxidative folding in eukaryotes.[10−19] The presence of redox-sensitive regulatory mechanisms affecting the activities of Ero1-Lα and potentially peroxiredoxin 4[20−25] suggests redox homeostasis is actively maintained in the ER.

A major obstacle in understanding the regulation of the ER redox environment is the difficulty in monitoring physiologically relevant changes in the ER redox potential in living cells. Until recently, real-time studies of the ER redox state have been impossible. Initial attempts to measure the ER redox state depended on the uptake of a labeled peptide that contains a cysteine and a glycosylation site into cultured mammalian cells.[26] The ER redox state was determined by recovery of the peptide and analyzing the oxidation state of the cysteine and sensitivity to specific endoglycosidases for ER localization.[26] This study showed that the couple of oxidized glutathione (GSSG) and reduced glutathione (GSH) is the major redox buffer in the secretory pathway with approximate reduction potentials of −170 to −180 mV and −133 to −165 mV, respectively, based on total glutathione concentrations of 8 and 1 mM, respectively.[26] A similar GSH:GSSG molar ratio of 3:1 was obtained by directly measuring monobromobimane-derived glutathione in rat liver microsomes.[27] However, a separate study of iodoacetic acid-treated rat liver microsomes

Received: January 12, 2013
Revised: April 2, 2013
Published: April 17, 2013

   dx.doi.org/10.1021/bi400052u | *Biochemistry* 2013, 52, 3332−3345

reported a higher GSH:GSSG ratio corresponding to a lower reduction potential of −205 mV.[28] Consistent with this observation, a significant amount of microsomal glutathione has been found as mixed protein disulfides;[27] however, the extent of glutathionylation is disputed.[28]

The ratiometric and redox-sensitive green fluorescent protein (roGFP) has been used to assess changes in the ER redox state in budding yeast[29] and cultured mammalian cells.[30] With midpoint potentials lower than −280 mV, these roGFP1- and roGFP2-based ER sensors allowed detection of reducing changes in the ER redox state but did not respond to oxidizing treatments.[29,30] More recently, two different redox sensors with higher midpoint reduction potentials have been introduced to monitor the ER redox state.[31−33] One of these sensors is derived from a new family of ratiometric roGFPs with an insertion (roGFP1-iX) that makes disulfide bonding less favorable and leads to higher reduction potentials (−229 mV for the most oxidizing member, roGFP1-iL).[34] The other sensor, based on Förster resonance energy transfer (FRET) between cyan and yellow fluorescent proteins in a manner dependent on the redox-mediated conformational change of a linker peptide, has an even higher reduction potential of −143 mV.[35] Analyses of the ER redox state using these two different sensors yielded values that were widely different from each other, and each was also different from prior estimates determined using the traditional biochemical and cell biology techniques described above. One study using roGFP1-iL and roGFP-iE targeted to the ER of the yeast *Pichia pastoris*[31] estimated an ER redox potential of approximately −230 mV,[31] a finding consistent with other studies showing the ability of roGFP1-iL to respond to both oxidizing and reducing treatments in human sarcoma cell line HT1080[33] and Chinese hamster ovary (CHO) cells.[32] In contrast, the FRET-based sensor remained mostly oxidized in the ER of CHO cells despite having an exceptionally high reduction potential of −143 mV, suggesting a glutathione potential of −118 mV at pH 7.[32]

Our work with the antidiabetic adipocyte hormone adiponectin indicates the assembly of higher-molecular weight complexes *in vitro* strongly depended on the redox environment.[36−38] To determine if the same holds true *in vivo*, we targeted the roGFP1-iL sensor to the ER (termed eroGFP1-iL by convention) of 3T3-L1 fibroblasts, a cell line that expresses adiponectin upon differentiation into adipocytes.[39] We were able to confirm that eroGFP1-iL responded to diamide-induced oxidizing changes,[31−33] suggesting much of eroGFP1-iL exists in the reduced state under basal conditions. Also similar to a prior study,[33] much of eroGFP1-iL was found as covalent dimers in the ER. Here we show that the dimer form of roGFP1-iL exhibited an intermediate excitation fluorescence spectrum between those of oxidized and reduced monomers. In addition, we found formation of the roGFP1-iL dimer was markedly enhanced in glutathione-based redox buffer, and the presence of the dimer effectively increased the reduction potential of roGFP1-iL. We conclude glutathione alters the redox state of roGFP1-iL in the ER through dimerization of the sensor, thereby allowing it to detect oxidizing changes. The results indicate that the determination of ER reduction potential using fluorescence-based sensors must be conducted to ensure the reduction potential of the sensor *in vivo* matches that measured *in vitro*.

MATERIALS AND METHODS

Generation of 3T3-L1 Fibroblasts Expressing eroGFP1-iL. To target roGFP1-iL[34] to the ER, polymerase chain reaction (PCR) was performed using roGFP1-iL as a template to remove the six-His tag and to engineer the signal peptide from mouse adiponectin[39] and the HDEL ER retention motif to the N- and C-termini of roGFP1-iL, respectively. The primers for the PCR contain the following sequences: upstream, 5′-GCGGATCCGCCACCATGCTACTGTTGCA-AGCTCTCCTGTTCCTCTTAATCCTGCCCAGTCATGC-CGAAGATAGTAAAGGAGAAGAACTTTTCACTGG-3′; and downstream, 5′-GGCGGTCGACTATTAGAGCTCATC-ATGTTCCGAATTCAGATCCTCTTCTGAGATGAGTTT-TTGTTCTTTGTATAGTTCATCCATGCCATGTGT-3′. The *myc* epitope tag was inserted between roGFP1-iL and the C-terminal HDEL motif as a spacer to promote the accessibility of the retention signal.[40] Following the established convention,[29] the roGFP1-iL construct containing the modifications described above is named eroGFP1-iL. Following digestion with *Bam*HI and *Sal*I restriction enzymes, the eroGFP1-iL PCR fragment was cloned into a similarly treated pBabe-puro vector (Addgene, Cambridge, MA). The resulting pBabe-eroGFP1-iL plasmid was cotransfected with pCL-Eco[41] into HEK 293T cells as described previously[42] to generate replication-deficient retrovirus. 3T3-L1 fibroblasts (ATCC, Manassas, VA) were infected according to protocols published on G. Nolan's Web site at Stanford University (http://www.stanford.edu/group/nolan/index.html) using conditioned medium collected from transfected HEK 293T cells after centrifugation at 1000*g* for 10 min and passage through 0.45 μm bottle-top filters. After 2 days, infected 3T3-L1 fibroblasts were selected in 6 μg/mL puromycin for 4 days.

Selection of Cells Expressing eroGFP1-iL Using Flow Cytometry. Puromycin-resistant 3T3-L1 fibroblasts infected with replication-defective retrovirus carrying eroGFP1-iL in the pBabe-puro vector were trypsinized, washed in phenol red-free RPMI 1640 medium with 2% BSA, and resuspended in the same medium for flow cytometry in FACSAria IIu (BD Biosciences, San Jose, CA). To avoid enrichment of cells exhibiting an abnormally high or low ER redox state, the cells were excited with a 488 nm laser and emission fluorescence was detected through a 530/30 bandpass filter. Even though roGFP1-iL absorbs poorly at 488 nm, the fluorescence emitted at that excitation wavelength was independent of the roGFP1-iL redox state.[34] Cells with a mean fluorescence in the top tenth percentile and cells in the next tenth percentile were sorted, expanded in culture, and analyzed for signs of ER stress.

Confocal Microscopy. 3T3-L1 fibroblasts expressing eroGFP1-iL were grown on glass coverslips in six-well plates, washed in PBS^{++} (phosphate-buffered saline with 0.9 mM $CaCl_2$ and 0.5 mM $MgCl_2$) with 0.2% BSA, and fixed in PBS^{++} with 4% paraformaldehyde. Permeabilization was performed for 10 min in PBS^{++} with 0.2% Triton X-100 at 40 °C followed by blocking in PBS^{++} with 2% BSA and 4% goat serum for 30 min at room temperature. Cells were stained sequentially using the 9B11 monoclonal antibody (Cell Signaling Technology, Inc., Danvers, MA) against the myc epitope tag followed by the Alexa Fluor 488-conjugated anti-mouse antibody (Invitrogen) and a polyclonal antibody (Cell Signaling Technology) against protein disulfide isomerase (PDI) followed by the Cy5-conjugated anti-rabbit antibody (Jackson ImmunoResearch, West Grove, PA). Staining with primary and secondary

antibodies was performed for 120 and 45 min, respectively, at room temperature in PBS^{++} with 2% BSA. After being stained, the samples were washed four times with PBS. Finally, the coverslips were sealed, imaged using a Nikon C1si scanning confocal microscope, and analyzed with EZ-C1.

ER Redox-State Measurement Using Epifluorescence Microscopy. 3T3-L1 fibroblasts were grown on 25 mm round No. 1 coverslips (VWR International, LLC) in six-well plates. To evaluate fluorescence, a coverslip was placed in a chamber held at 37 °C while mounted on the stage of an inverted Olympus IX70 microscope equipped with a 40× 1.4 NA ultrafluorophore objective. The oxidized and reduced forms of eroGFP1-iL were maximally excited by light from a 100 W mercury lamp through 380 ± 5 and 455 ± 15 nm bandpass filters, respectively. A computer-controlled filter wheel was used to rotate the excitation filters allowing for a pair of images to be acquired within approximately 5 s. The emission filter had a 10 nm bandwidth centered at 510 nm. Because light exposure drives eroGFP1-iL to its oxidized state,[33] the excitation source was shuttered, and the exposure time was minimized (1 s per image). Prior to being mounted on a microscope, cells on coverslips were incubated for 2 h in fresh normal growth medium (DMEM supplemented with 10% calf serum, 2 mM L-glutamine, 100 units/mL penicillin, and 100 μg/mL streptomycin) followed by 1 h in phenol red-free RPMI 1640 medium supplemented with 2% Fraction V BSA (Research Products International, Mt. Prospect, IL), 2 mM L-glutamine, and 20 mM Hepes (pH 7.4). To initiate an experiment, the stimulated fluorescence was recorded at 5 min intervals until a steady-state fluorescence was reached. Subsequently, cells were treated with diamide (VWR International, LLC) or dithiothreitol (DTT) (Sigma-Aldrich, St. Louis, MO), and images were acquired at fixed intervals. The fluorescence intensity was quantified using ImageJ. Specifically, all of the images collected from one coverslip including the baseline were first collated into a stack, and on average, eight box-shaped regions of interest (ROIs) encompassing areas of varying fluorescence intensities and three background ROIs were drawn per stack of images. Intensities of the same box on successive images within the stack were reduced by the average intensities of the background boxes. Background-subtracted ROI intensities on the images collected through the 380 ± 5 nm bandpass filter were divided by similarly adjusted intensities of the same ROIs on the corresponding images collected through the 455 ± 15 nm filter to obtain a ratio of oxidized to reduced eroGFP1-iL within a given ROI. This procedure was modified when some of the images within a stack varied slightly, a situation encountered from time to time in which fluorescent areas of cells decreased upon prolonged exposure to diamide. In this case, a freehand tool was used to draw ROIs that each encompass the largest fluorescent area of a cell among all images within a stack. These areas almost always contain nuclei without green fluorescence, and the oval tool was used to draw nucleus-encompassing ROIs that were intersected out of the areas surrounding the ER. The resulting ROIs were duplicated and moved to regions of the image without green fluorescence to serve as background. In all cases, the background-adjusted emission fluorescence intensity following excitation at 380 nm (maximum for oxidized roGFP1-iL) was divided by that at 455 nm (maximum for reduced roGFP1-iL) to obtain a 380 nm/455 nm fluorescence intensity ratio, which was then normalized to that of the baseline before treatment. By the established convention,[29] the term "eroGFP1-iL ratio" is defined as $\log_2$ values of the baseline-normalized 380 nm/455 nm fluorescence ratio. The rationale for transforming baseline-normalized 380 nm/455 nm fluorescence ratios to $\log_2$ space, used to represent increasingly oxidized eroGFP1-iL, is presented as positive values, while increasing amounts of reduced eroGFP1-iL are presented as negative values.

ER Redox-State Measurement Using Flow Cytometry. 3T3-L1 fibroblasts were maintained in normal growth medium (defined above) at 37 °C until >70% confluence was reached. Cells were replenished with fresh normal growth medium for 2 h and then transferred to phenol red-free RPMI 1640 supplemented with 2% Fraction V BSA, 2 mM L-glutamine, and 20 mM Hepes (pH 7.4) for 1 h at 37 °C prior to the addition of 1 mM diamide or 1 mM DTT and further incubation at 37 °C for 5 and 15 min. Cells were then scraped from culture plates, passed through 40 μm cell strainers, and excited sequentially with a 405 nm laser for maximal emission by oxidized eroGFP1-iL and a 488 nm laser for redox-independent eroGFP1-iL fluorescence in an LSR II flow cytometer (BD Biosciences). Fluorescence generated by both lasers was detected through a 520/50 bandpass filter with a 505 nm long-pass dichroic mirror. Data acquisition and analysis were performed using FACSDiva (BD Biosciences). Fibroblasts were gated away from debris and aggregates based on forward versus side scatter. Proportions of oxidized eroGFP1-iL relative to total eroGFP1-iL were represented by ratios of mean fluorescence from excitation at 405 nm to that from excitation at 488 nm. After normalization to untreated control cells, the 405 nm/488 nm mean fluorescence ratios were transformed into $\log_2$ space to set controls to zero and oxidizing and reducing changes to positive and negative values, respectively, of comparable scales.

Nonreducing Denaturing Immunoblot Analysis of eroGFP1-iL Redox States. 3T3-L1 fibroblasts expressing eroGFP1-iL on 10 cm culture plates were transferred to fresh normal growth medium 2 h prior to treatment with either 1 mM diamide or DTT for 5 and 15 min. At the end of the incubation, media were aspirated and the cells were washed once with ice-cold PBS followed by precipitation in 700 μL of ice-cold 10% trichloroacetic acid (TCA) for 5 min. The precipitates were scraped off of the plates and centrifuged at 4 °C and 2700*g* for 10 min. After removal of the supernatant, the pelleted precipitates were washed three times with ice-cold 70% acetone and air-dried. The pellets were then resuspended in 20 mM *N*-ethylmaleimide (NEM), 10% SDS, and 5 mM Hepes (pH 7.4) and incubated on ice for 20 min followed by constant vortexing for 90 min at room temperature. Laemmli sample loading buffer[43] without reducing agent was added, and the samples were heated for 15 min at 90 °C prior to fractionation in 10% Tris-glycine gels. Following electrophoretic transfer, nitrocellulose membranes were stained with Ponceau S, blocked, and incubated with antibodies against the *myc* epitope or β-actin (Cell Signaling Technology, Danvers, MA) followed by horseradish peroxidase-conjugated goat anti-mouse and donkey anti-rabbit IgG (Jackson ImmunoResearch). Blots were developed using enhanced chemiluminescence (Thermo Scientific, Rockford, IL) and visualized in a Chemidoc XRS imaging system (Bio-Rad Laboratories, Philadelphia, PA).

Expression and Purification of roGFP1-iL and A206K roGFP1-iL. Six-His-tagged roGFP1-iL in the pQE30 vector was a gift from S. James Remington.[34] Expression and purification were performed essentially as described previously with modifications.[34] Protein was expressed in BL21(DE3)pLysS

cells after induction with 1 mM ITPG at 37 °C for 4 h. The cell lysate supernatant was loaded onto a nickel-charged HiTrap chelating column (GE Healthcare, Pittsburgh, PA) and eluted with a step imidazole gradient. roGFP1-iL was purified to homogeneity with an additional anion exchange chromatography step using quaternary ammonium resin and elution with a continuous NaCl gradient from 50 to 500 mM. Purified protein was dialyzed into PBS, sterile-filtered, and stored at 4 °C. An A206K amino acid substitution was introduced into roGFP1-iL in pQE30 using QuikChange mutagenesis in two stages. First, the GCC codon corresponding to alanine was changed to AAC. A second round of PCR-based mutagenesis was then performed to change AAC to the lysine-encoding AAA sequence.

Redox Titration of roGFP1-iL *in Vitro* and Fluorescence Spectroscopy. For titration in mono- and dithiol redox buffers, a total of 2.5 mM reduced and oxidized glutathione ([GSH] + 2[GSSG] = 2.5 mM) or DTT ([DL-dithiothreitol] + [*trans*-4,5-dihydroxy-1,2-dithiane] = 2.5 mM) was combined in 20 mM Hepes, 150 mM NaCl, and 1 mM EDTA (pH 7.0) to generate buffers with the indicated redox potentials using the Nernst equation and values of −230 and −330 mV for standard reduction potentials of glutathione and DTT, respectively. roGFP1-iL was added to a final concentration of 7.5 μM. Reaction tubes were sealed with rubber septa, and nitrogen gas was passed through the reaction tubes for 1 min. The reaction mixtures were incubated at 37 °C in the dark for 4 h prior to the determination of excitation fluorescence spectra and redox state by nonreducing SDS−PAGE. Excitation spectra were determined using Varioskan Flash fluorescence plate reader (Thermo Scientific, Hudson, NH) or model 8000 SLM Aminco T-format spectrofluorometer (SLM Instruments, Urbana, IL). Excitation scans from 350 to 490 nm were taken with emission measured at 510 ± 20 nm. Excitation spectra were normalized to the isosbestic point of roGFP1-iL at 429 nm (data not shown). Fluorescence intensities at specific wavelengths were relative to that at 429 nm, which is arbitrarily set to 1. For titration in diamide, 15 μM roGFP1-iL was incubated for 30−60 min at room temperature in either PBS or 20 mM Hepes, 150 mM NaCl, and 1 mM EDTA (pH 7.0) prior to nonreducing denaturing gel electrophoresis.

Assessment of the roGFP1-iL Redox State *in Vitro* by Nonreducing SDS−PAGE. Following incubation in DTT- or glutathione-based redox buffers and determination of excitation fluorescence spectra, roGFP1-iL samples were quenched with 25 mM NEM for 10 min at room temperature followed by denaturation in Laemmli sample loading buffer[43] without a reducing agent by being heated to 90 °C for 15 min. Samples were fractionated in 10% Tris-glycine, 4−12% Bis-Tris, or 10% Bis-Tris gels and stained with Coomassie Brilliant Blue G-250. Quantitation of images was performed using ImageJ following digitization in an Epson Perfection 4990 optical scanner or a LI-COR Odyssey infrared imaging system (LI-COR Biosciences, Lincoln, NE) as previously described.[44]

Gel Filtration Chromatography. roGFP1-iL dimers and monomers were separated on a Superdex 75 column (GE Healthcare Biosciences, Piscataway, NJ). The column was equilibrated and eluted in 20 mM Hepes, 150 mM NaCl, and 1 mM EDTA (pH 7.0) at 1 mL/min at room temperature. Fractions (0.2 mL) were collected and analyzed by nonreducing SDS−PAGE and fluorescence spectroscopy.

Molecular Modeling of roGFP1-iL Dimers. Molecular modeling of roGFP1-iL dimers was performed using MODELLER software module.[45] Structural templates to which the roGFP1-iL sequences were aligned were 2B3Q, a crystallized dimer of GFP,[46] and two copies of 3CBE, roGFP1-*iR* in the reduced conformation.[34]

Statistical Analysis. Data are presented as means ± the standard deviation. Statistical comparisons between groups with roGFP1-iL under different treatment conditions were performed using either a paired or an unpaired Student's *t* test with two tails. Statistical comparison of eroGFP1-iL ratio was evaluated using a one-sample, two-tailed, *t* test against the expected value of 0. The particular statistical analyses applied to the results in specific experiments are described in figure legends. All experiments were performed at least three times.

RESULTS

Generation of a Stable Cell Line Expressing eroGFP1-iL in the ER. To generate an ER-specific redox reporter, the signal peptide sequence from mouse adiponectin cDNA[47] and a *myc* epitope tag ending in ER retention motif HDEL were attached to the N- and C-termini, respectively, of the previously characterized roGFP1-iL ratiometric sensor.[34] The resulting eroGFP1-iL construct was stably introduced into 3T3-L1 fibroblasts (3T3-L1-eroGFP1-iL cells) as described in Materials and Methods. To examine if eroGFP1-iL is localized to the ER, we assessed the degree of colocalization between eroGFP1-iL and protein disulfide isomerase (PDI) using laser-scanning confocal microscopy following staining of fixed 3T3-L1 fibroblasts using antibodies against the *myc* epitope tag and PDI. As shown in Figure 1A, there was a near complete overlap between signals produced by eroGFP1-iL and PDI (Pearson's correlation and Mander's overlap coefficients of 0.96 ± 0.02 and 0.97 ± 0.01, respectively, over nine different fields). As overexpression of proteins in the ER could lead to induction of an unfolded protein response, we assessed if 3T3-L1-eroGFP1-iL fibroblasts exhibited ER stress. Although roGFP1-iL emits poorly when excited by 488 nm light, 3T3-L1-eroGFP1-iL cells nevertheless showed higher fluorescence than control cells with the pBabe-puro vector (Figure 1B). Populations of cells with eroGFP1-iL fluorescence in the top tenth percentile and the next tenth percentile were separated by flow cytometry (Figure 1C) and expanded, and immunoblot analysis was performed to determine the levels of eroGFP1-iL (Figure 1D) and the ER stress marker BiP (Figure 1E). In contrast to 3T3-L1 fibroblasts treated with 1 μM thapsigargin, no evidence of BiP induction was observed in the 10 and 20% of the cells expressing the highest levels of eroGFP1-iL.

Changes in eroGFP1-iL Fluorescence following Treatments with Oxidizing and Reducing Agents. To determine if 3T3-L1-eroGFP1-iL fibroblasts can respond to changes in the redox state, cells mounted on a heated epifluorescence microscope stage maintained at 37 °C were treated with 1 mM diamide or DTT. Live cell fluorescence images were first acquired for untreated cells to obtain the baseline redox condition. Cells were then treated with diamide or DTT and imaged after 1, 5, 10, and 15 min to obtain the eroGFP1-iL ratio, a term defined in Materials and Methods in depth as the $\log_2$ value of fluorescence excited at 380 nm versus that at 455 nm normalized to baseline. Treatment with diamide led to an increase in the eroGFP1-iL ratio from 0 to 0.63 ± 0.09 within the first minute (Figure 2A,B). DTT brought about an immediate reduction in the eroGFP1-iL ratio, with the most dramatic response occurring also in the first minute (Figure 3A,B). Maximal changes in eroGFP1-iL ratios following both

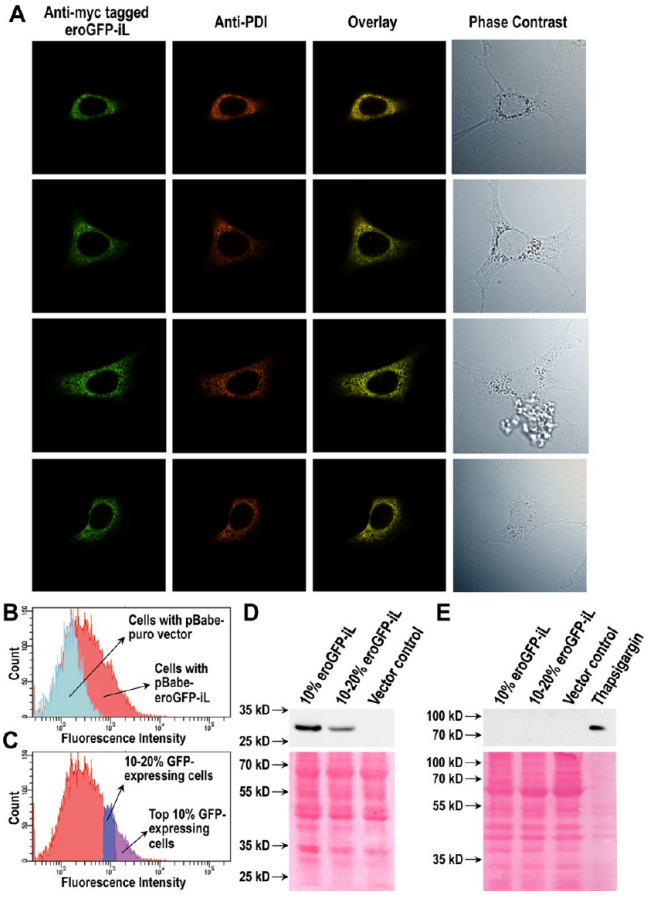

Figure 1. Assessment of colocalization of PDI and myc epitope-tagged eroGFP1-iL in 3T3-L1-eroGFP1-iL fibroblasts by confocal microscopy (A) and concentration of the ER stress marker BiP in 3T3-L1 fibroblasts expressing varying amounts of eroGFP1-iL (B–D). (A) Representative phase contrast and confocal fluorescence microscopy images of 3T3-L1-eroGFP1-iL cells stained with antibodies against the myc epitope and PDI followed by Alexa Fluor 488- and Cy5-conjugated secondary antibodies, respectively. (B) Fluorescence of 3T3-L1 fibroblasts infected with replication-defective retrovirus carrying the eroGFP1-iL construct or vector assessed by flow cytometry (488 nm excitation, 530 ± 15 nm emission) and plotted as a histogram. (C) Fluorescence of 3T3-L1-eroGFP1-iL fibroblasts determined by flow cytometry (488 nm excitation, 530 ± 15 nm emission) and plotted as a histogram showing the top tenth percentile and the next tenth percentile of cells with the highest fluorescence. (D and E) Immunoblot analyses of 3T3-L1-eroGFP1-iL cells sorted for being in the top 10% and the top 10–20% of cells with the highest fluorescence, 3T3-L1 cells carrying the pBabe-puro vector as a negative control, and thapsigargin-treated 3T3-L1 fibroblasts as a positive control for the (D) *myc* epitope tag and (E) ER stress marker BiP.

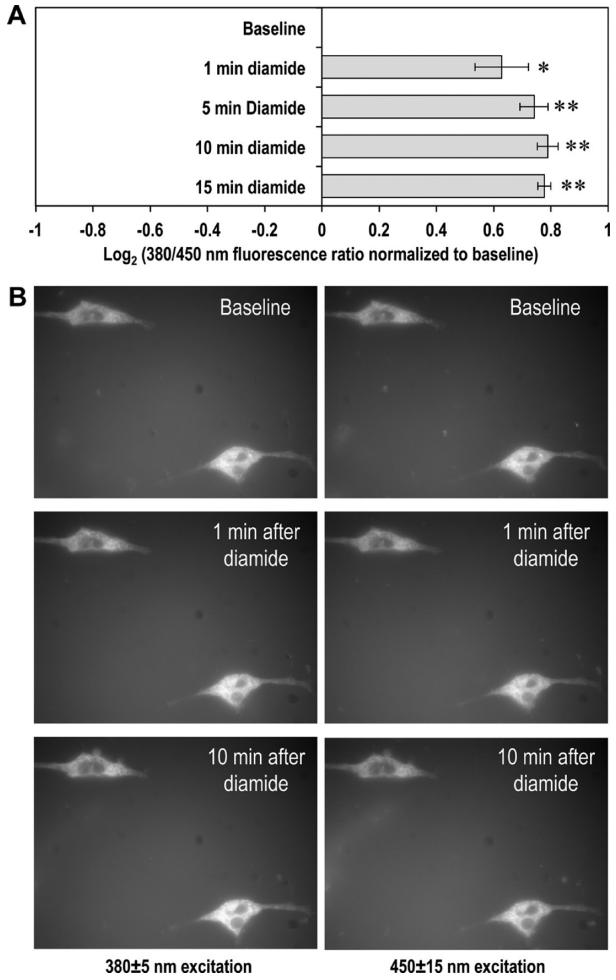

Figure 2. Real-time changes in the fluorescence of 3T3-L1-eroGFP1-iL fibroblasts monitored using epifluorescence microscopy at baseline and after treatment with 1 mM diamide for 1, 5, 10, and 15 min at 37 °C. (A) eroGFP1-iL ratio ($\log_2$ values of baseline-normalized 380 nm/455 nm fluorescence ratios, described in greater detail in Materials and Methods) averaged from four independent experiments after diamide treatment. One asterisk and two asterisks denote $p < 0.01$ and $p < 0.001$, respectively, in a one-sample, two-tailed, t test against an expected value of 0. (B) Representative epifluorescence images of 3T3-L1-eroGFP1-iL cells at baseline and after treatment with diamide for 1 and 10 min. Cells were excited with light from a mercury lamp through a 380 ± 5 nm bandpass filter (left) or a 455 ± 15 nm bandpass filter (right), and epifluorescence was collected through a 510 ± 10 nm bandpass filter.

DTT and diamide treatments were observed at the end of 10 min (Figures 2A and 3A). While Figures 2B and 3B depict only images at baseline and after treatments for 1 and 10 min, fluorescence changes across all time points are shown as QuickTime movies in Figure S1 of the Supporting Information. Although in opposite directions, the maximal changes in eroGFP1-iL ratios from baseline were approximately equal in absolute terms for DTT and diamide treatments [0.72 ± 0.1 and 0.79 ± 0.04, respectively (Figures 2A and 3A)].

To assess the robustness of the ability of eroGFP1-iL to detect redox changes, cells treated with diamide or DTT were analyzed using flow cytometry with only a 405 nm laser to excite the fluorophore in a redox-sensitive manner and a 488 nm laser to excite it in a redox-independent fashion. 3T3-L1-eroGFP1-iL cells grown on culture plates were treated with 1 mM diamide or 1 mM DTT for 5 and 15 min. At the end of the treatment, cells were collected and subjected to flow cytometric analysis as described in Materials and Methods. A statistically significant oxidizing change in the ER, measured as the $\log_2$ ratio of intensities of light emitted by the oxidized eroGFP1-iL following excitation at 405 and 488 nm, was recorded after diamide treatment for 15 min [0.27 ± 0.06 (Figure 4A,B)]. Similarly, significant decreases in the $\log_2$ ratio of 405 nm to 488 nm fluorescence intensities were observed after DTT treatment for 5 and 15 min [−0.41 ± 0.04 and −0.40 ± 0.02, respectively (Figure 4A,C)].

Redox States of eroGFP1-iL in 3T3-L1 Fibroblasts in Response to Diamide and DTT. To evaluate the physical

dx.doi.org/10.1021/bi400052u | *Biochemistry* 2013, 52, 3332–3345

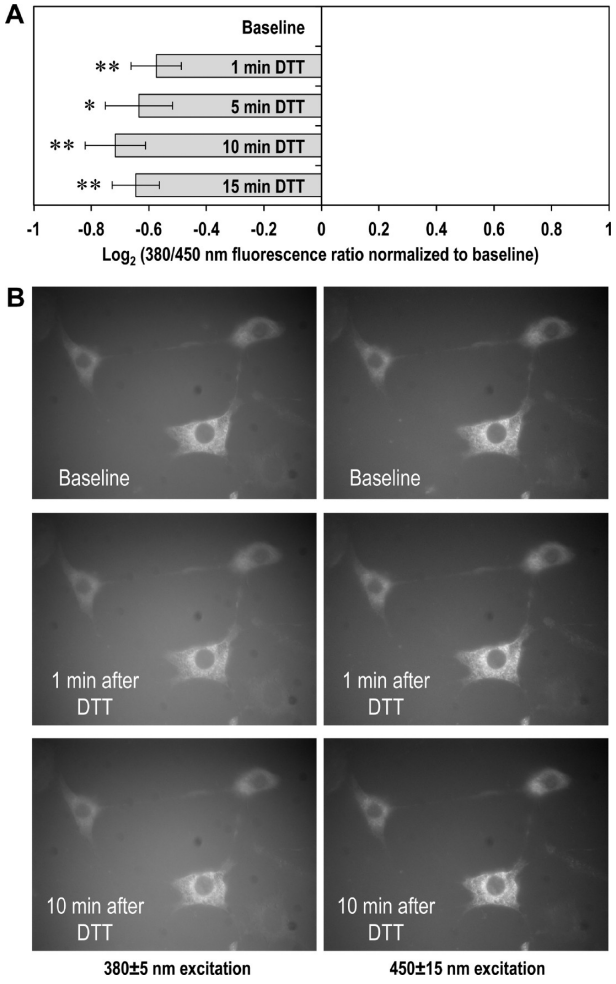

Figure 3. Real-time changes in the fluorescence of 3T3-L1-eroGFP1-iL fibroblasts monitored using epifluorescence microscopy at baseline and after treatment with 1 mM DTT for 1, 5, 10, and 15 min at 37 °C. (A) eroGFP1-iL ratio (log_2 values of baseline-normalized 380 nm/455 nm fluorescence ratios, described in greater detail in Materials and Methods) averaged from four independent experiments after DTT treatment. One asterisk and two asterisks denote $p < 0.03$ and $p < 0.01$, respectively, in a one-sample, two-tailed, t test against an expected value of 0. (B) Representative epifluorescence images of 3T3-L1-eroGFP1-iL cells at baseline and after treatment with DTT for 1 and 10 min. Cells were excited with light from a mercury lamp through a 380 ± 5 nm bandpass filter (left) or a 455 ± 15 nm bandpass filter (right), and epifluorescence was collected through a 510 ± 10 nm bandpass filter.

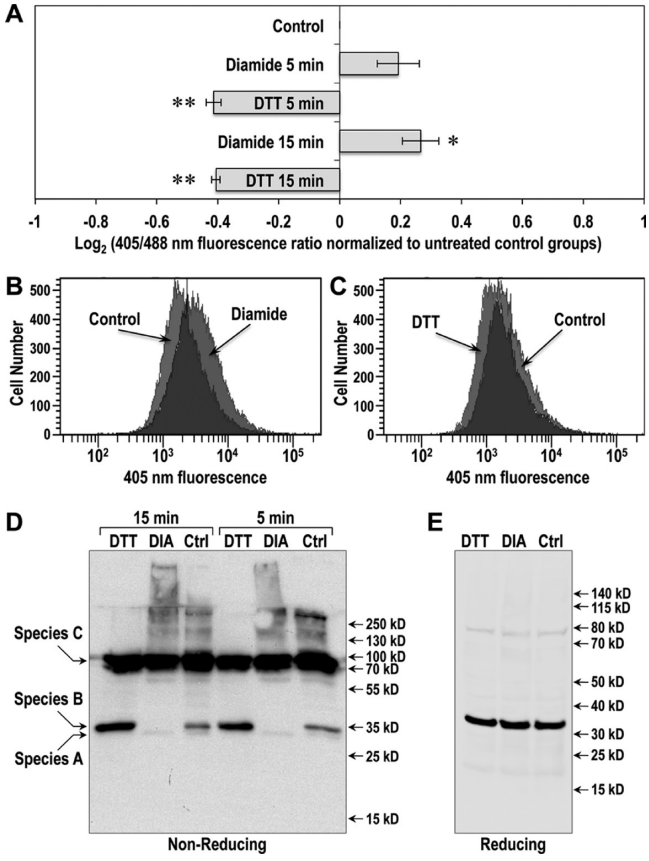

Figure 4. Response of eroGFP1-iL to oxidizing and reducing agents measured using only one redox-sensitive excitation wavelength (A–C) and immunoblot analysis of eroGFP1-iL redox states (D and E). Relative amounts of oxidized eroGFP1-iL in 3T3-L1-eroGFP1-iL cells after diamide or DTT treatment for 5 and 15 min were measured using flow cytometry by normalizing the 405 nm laser-excited mean fluorescence intensity with that excited by a 488 nm laser because both oxidized and reduced roGFP1-iL exhibited equal fluorescence intensities upon excitation at 488 nm.[34] The bar graph in panel A shows the 405 nm/488 nm laser-excited mean fluorescence intensity ratios normalized to untreated controls and expressed on a log_2 scale. Values were averaged from three independent experiments with a minimum of 7500 events per sample. One asterisk and two asterisks denote $p < 0.05$ and $p < 0.005$, respectively, in a one-sample, two-tailed, t test against an expected value of 0. (B and C) Representative flow cytometry histograms plotting the cell number against the green fluorescence of untreated 3T3-L1-eroGFP1-iL fibroblasts and either (B) diamide-treated or (C) DTT-treated cells (15 min at 37 °C) following excitation with a 405 nm laser. Redox states of eroGFP1-iL in untreated and either diamide- or DTT-treated 3T3-L1 fibroblasts were determined using antibodies against the myc epitope to probe Western blots of TCA-precipitated cell lysates resolved via (D) nonreducing and (E) reducing SDS–PAGE. 3T3-L1-eroGFP1-iL cells treated with or without 1 mM diamide or 1 mM DTT for 5 and 15 min were precipitated with 10% TCA followed by resolubilization in the presence of 20 mM NEM to protect redox states. The blot shown is representative of five independent experiments. For reducing SDS–PAGE, resolubilized TCA precipitates in sample loading buffer were heated for 15 min at 90 °C in the presence of 100 mM βME prior to loading.

state of the eroGFP1-iL protein *in vivo* upon treatment with oxidizing and reducing agents, 3T3-L1-eroGFP1-iL cells were incubated with 1 mM diamide or DTT for 5 and 15 min at 37 °C and then precipitated with TCA followed by resolubilization in SDS and NEM to preserve redox states. Samples were fractionated via nonreducing SDS–PAGE, transferred to nitrocellulose, and probed with an antibody against the myc epitope tag located on the C-terminus of eroGFP1-iL. We observed three distinct species of eroGFP1-iL that are labeled A–C in Figure 4D. Species A and B had molecular weights corresponding to that of monomeric eroGFP1-iL. Species A migrated faster than species B and is thus consistent with it being the oxidized form of the eroGFP1-iL monomer containing a disulfide bond between C147 and C204. Species B is most likely the reduced form of the eroGFP1-iL monomer without a disulfide bond to constrain its conformation during nonreducing SDS–PAGE. In untreated 3T3-L1-eroGFP1-iL fibroblasts, both oxidized and reduced monomers of eroGFP1-iL were found with larger amounts of reduced monomers versus oxidized monomers (Figure 4D). Upon diamide

dx.doi.org/10.1021/bi400052u | *Biochemistry* 2013, 52, 3332–3345

treatment, the reduced eroGFP1-iL monomers (species B) disappeared, but oxidized monomers did not (species A and Figure 4D). Levels of reduced monomers (species B) increased, and oxidized monomers (species A) disappeared upon DTT treatment (Figure 4D). Species C was the predominant form of eroGFP1-iL in cells under all conditions (Figure 4D). As the presence of βME in sample loading buffer almost completely eliminated the presence of species C (Figure 4E), this species is most likely a disulfide-bonded homodimer of eroGFP1-iL or a disulfide-bonded heterodimer between eroGFP1-iL and another protein with a similar molecular weight. A reducing agent-collapsible ER roGFP1-iL band with an apparent molecular weight similar to that of species C in nonreducing SDS−PAGE has been observed previously in HT1080 cells,[33] indicating species C is not an artifact specific to 3T3-L1 fibroblasts.

Presence of Redox-Sensitive roGFP1-iL Dimers *in Vitro*. To determine if species C in nonreducing immunoblot analysis could be a dimer of eroGFP1-iL, we examined if purified roGFP1-iL formed dimers *in vitro*. Purified roGFP1-iL containing a mixture of oxidized and reduced monomers and small amounts of dimers were treated with 0, 0.5, 5, or 10 mM diamide for 2 h at room temperature to determine if an oxidizing environment could facilitate dimer formation. Addition of diamide led to the conversion of monomers to dimers (Figure 5A) that was manifested by an increased ratio of dimers to monomers (Figure 5B). Interestingly, conversion to dimers was most robust at 0.5 mM diamide (Figure 5A), leading to the highest dimer/monomer ratio at that concentration (Figure 5B). Paradoxically, the dimer/monomer ratio decreased progressively with an increasing diamide concentration (Figure 5B).

Molecular Modeling of the roGFP1-iL Dimer. To assess how roGFP1-iL monomers could interact to form a covalent dimer, homology models of the roGFP1-iL dimer were built using MODELLER software[45] with reduced roGFP1-*iR* (3CBE) and a crystallized GFP dimer (2B3Q) as model templates. MODELLER was able to generate disulfide-bonded dimers in both cross [C147−C204 and C204−C147 (Figure 5C,D)] and para [C147−C147 and C204−C204 (Figure 5E,F)] conformations that had highly similar DOPE energy values. Five successfully produced models for each of the two conformations are shown in Figure S2 of the Supporting Information, while the models with the lowest DOPE value in each conformation are shown in Figure 5C−F. C70, the third cysteine residue in roGFP1-iL, is located far from the dimer interface and is thus not likely to form disulfide bonds. The redox sensitivity of the entire roGFP1-iX family depends upon whether a disulfide bridge is present between C147 and C204 of the GFP monomer.[34] Formation of dimers mediated by disulfide bridges involving C147 and/or C204 residues suggests roGFP1-iL could exist in redox states in addition to oxidized or reduced monomers.

Decreased Level of Formation of the roGFP1-iL Dimer following Disruption of the Hydrophobic Region near C204. GFP forms weak dimers in solution with an approximate K_D of 100 μM,[48] and substituting alanine at position 206 with lysine further weakened the tendency to form dimers.[49] Examination of the crystal structure of roGFP1-iE showed the A206 residue forms part of a hydrophobic surface in the proximity of one of the redox-sensitive cysteine residues, C204 (Figure 6A,B). We hypothesized that if substituting A206 with a charged residue led to a decreased level of formation of disulfide-linked dimers, it will provide experimental support for

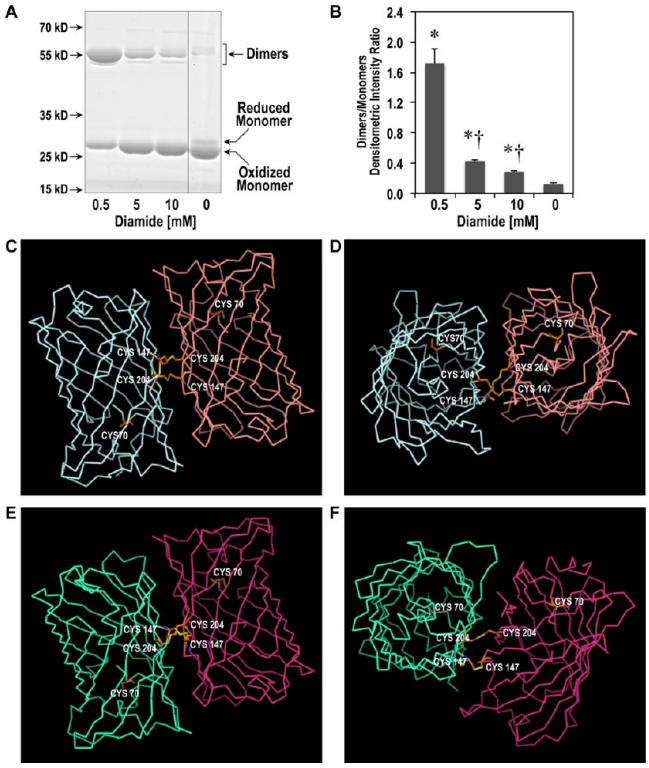

Figure 5. Redox-sensitive formation of roGFP1-iL dimers *in vitro* (A and B) and models of the roGFP1-iL dimer in (C and D) cross and (E and F) para conformations viewed from (C and E) sides and (D and F) ends of GFP's barrel-like structures. Representative nonreducing SDS−PAGE analysis of roGFP1-iL following incubation in 0, 0.5, 5, and 10 mM diamide is shown in panel A and the ratio of the intensities of dimers to monomers in panel B. Asterisks and daggers denote $p < 0.05$ in a Student's unpaired, two-tailed t test against groups with 0 and 0.5 mM diamide, respectively (n = 2−4 per group). Cα traces of roGFP1-iL dimers in cross and para conformations modeled using MODELLER and rendered in MacPyMol are shown in panels C−F. In the cross conformation, the C147 residue of one monomer forms a disulfide bond with the C204 residue of the other monomer and vice versa. In the para conformation, the C147 residue of one monomer forms a disulfide bond with the same residue on the other monomer while the other disulfide bond is between the C204 residues of adjacent monomers. C70, the third cysteine residue in roGFP1-iL, is also labeled.

C204 as one (or the only) cysteine residue in forming the disulfide bridge between two roGFP1-iL monomers. As shown in Figure 6C, roGFP1-iL with the A206K substitution exhibited a weakened tendency to form dimers as manifested in a lower dimer/monomer ratio (Figure 6D) in both reducing (−280 mV) and oxidizing (−160 mV) environments.

Excitation Fluorescence Spectrum of roGFP1-iL Dimers. As dimers represent a major portion of the total eroGFP1-iL found in 3T3-L1-eroGFP1-iL cells (Figure 4D), the dimers' fluorescence property must be determined to understand how the fluorescence of 3T3-L1-eroGFP1-iL cells changes in response to redox-active agents. Size exclusion chromatography was performed to separate dimers (fraction A in Figure 7A) from monomers (fraction B in Figure 7A) of roGFP1-iL. As fraction A remained contaminated with significant amounts of monomers, the sample was further treated with oxidized lipoic acid to increase the proportion of dimers (Figure 7B). For comparison, fraction A was also treated with DTT to convert all species to reduced monomers and

dx.doi.org/10.1021/bi400052u | *Biochemistry* 2013, 52, 3332−3345

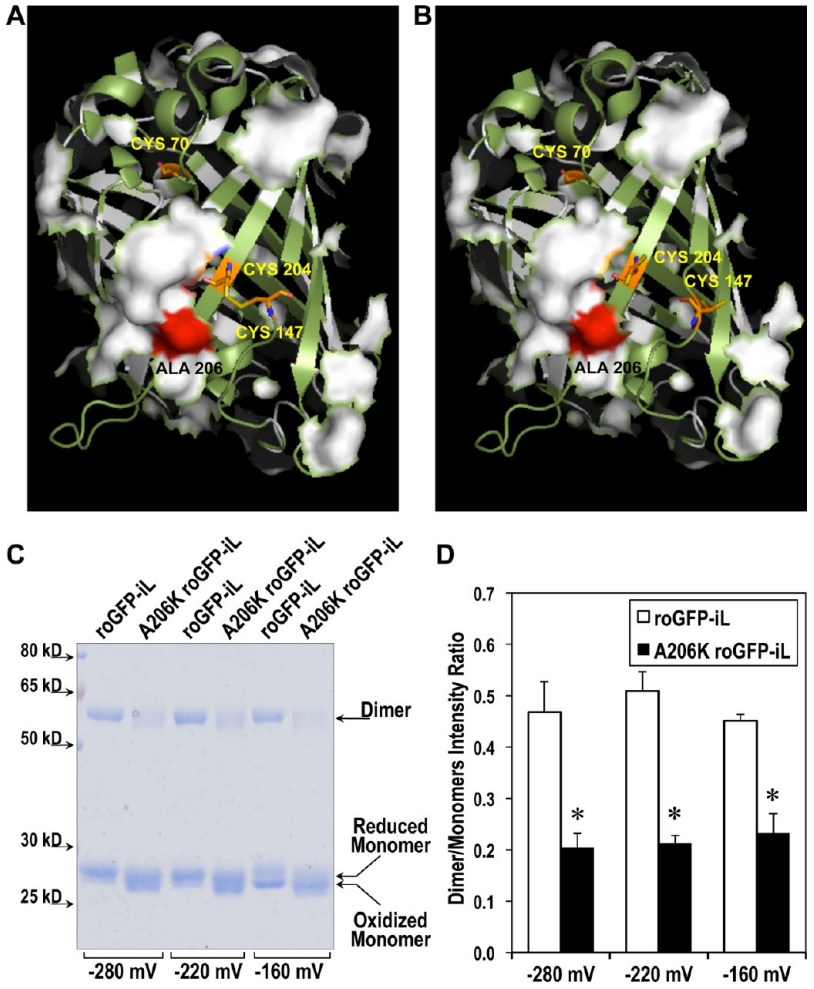

Figure 6. Ribbon diagrams of (A) oxidized and (B) reduced roGFP-iE with hydrophobic surface residues colored white, cysteine residues orange, and the alanine residue at position 206 red. (C) Representative Coomassie Brilliant Blue-stained nonreducing SDS−PAGE gel of purified roGFP1-iL and roGFP1-iL with a lysine residue substituted for alanine at position 206 (A206K roGFP1-iL) following incubation for 4 h in glutathione redox buffers at reduction potentials of −280, −220, and −160 mV. The abundance of roGFP1-iL dimers relative to that of combined reduced and oxidized monomers at each reduction potential was determined by densitometric analyses of the gels and is represented in panel D as the dimer/monomer intensity ratio in bar graph format. Results were averaged from three independent experiments, and an asterisk denotes $p < 0.05$ in a paired, two-tailed, Student's t test.

fraction B was found to consist exclusively of oxidized monomers (Figure 7B). As shown in Figure 7C, the excitation fluorescence spectra of fraction A and oxidized lipoic acid-treated fraction A were intermediate between those of reduced monomers (fraction A with DTT) and oxidized monomers (fraction B). These results indicate dimers of roGFP1-iL display an intermediate excitation fluorescence spectrum similar to having a mixture of oxidized and reduced monomers.

Increased roGFP1-iL Reduction Potential Caused by the Glutathione-Mediated Dimer. The intermediate fluorescence spectra of roGFP1-iL dimers may help to explain the ability of 3T3-L1-eroGFP1-iL cells to respond to both oxidizing and reducing changes (Figures 2 and 3). As a result, we assessed whether formation of the dimers is sensitive to differences in the redox environment by titrating roGFP1-iL in two different types of redox buffers, oxidized and reduced DTT (DTT/DTTox) and glutathione (GSH/GSSG). DTT/DTTox was used because it is a dithiol-based system similar to the oxidized and reduced lipoic acid used previously to determine the reduction potential of roGFP1-iL,[34] and GSH/GSSG is the major physiological redox buffer in ER.[26] It was observed that the excitation fluorescence spectra of roGFP1-iL were surprisingly different in DTT/DTTox (Figure 8A) and GSH/GSSG (Figure 8B) buffers. In DTT/DTTox, the fluorescence spectra indicated nearly 100% of roGFP1-iL existed in the oxidized state at −190 mV and above (Figure 8A). In GSH/GSSG, not until −100 mV were all of the roGFP-iL molecules oxidized (Figure 8B). The differences in fluorescence spectra between the two buffer systems were associated with a significantly weakened tendency for roGFP1-iL to dimerize in DTT/DTTox (Figure 8C) compared with GSH/GSSG (Figure 8D). At −340, −310, −280, −220, and −190 mV, the percentage of dimers as total roGFP1-iL was significantly higher in GSH/GSSG than in DTT/DTTox (Figure 8E). In addition to an increased level of dimer formation, another surprise is monomeric roGFP1-iL molecules in GSH/GSSG buffer were more easily reduced or more difficult to oxidize than the monomers in DTT/DTTox buffer (Figure 8C,D). While the midpoint reduction potential of the roGFP-iL monomer in DTT/DTTox was approximately −240 mV, that in GSH/GSSG was approximately −155 mV (Figure 8F). At −250, −220, −190, and −160 mV, the percentages of

dx.doi.org/10.1021/bi400052u | Biochemistry 2013, 52, 3332−3345

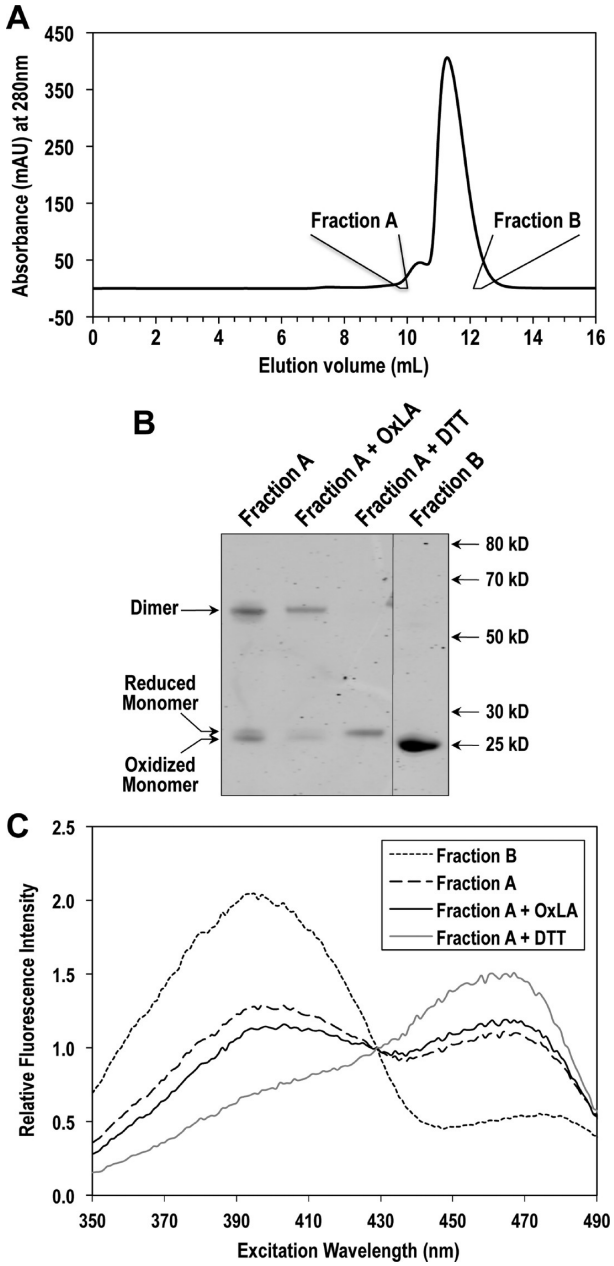

Figure 7. Enrichment of roGFP1-iL dimers for the determination of excitation fluorescence spectra. (A) Elution profile of roGFP1-iL in a Superdex 75 gel filtration column showing the two fractions, labeled A and B, that underwent further analyses. Aliquots of fraction A, fraction A treated with 100 mM oxidized lipoic acid (OxLA), fraction A treated with 10 mM DTT, and fraction B were analyzed using (B) nonreducing SDS–PAGE followed by staining with Coomassie Brilliant Blue and (C) excitation fluorescence spectroscopy with fixed emission at 510 ± 20 nm.

monomeric roGFP1-iL that were reduced were significantly higher in GSH/GSSG buffer than in DTT/DTTox buffer (Figure 8F).

DISCUSSION

Given the vital role of ER oxidative protein folding in cellular homeostasis, it is important to understand how redox state is regulated in that cellular compartment. Our current understanding of ER redox-state regulation is poor. A real-time sensor of the ER redox state will accelerate the discovery process. The commonly used roGFP1 has been targeted to the ER previously but was found to be able to detect only reducing changes in the ER,[29,30] presumably because of the large difference between the midpoint reduction potential of roGFP1 (approximately −280 mV) and the reduction potential of the glutathione couple in the ER measured using biochemical approaches (approximately between −160 and −200 mV).[26−28] Newer fluorescent sensors whose *in vitro* midpoint reduction potentials are closer to that in the ER have been developed recently and used to assess redox changes in the ER.[31−33] As detailed in the introductory section, results from these real-time fluorescence-based sensors conflict with the earlier results obtained using biochemical approaches. In this study, we uncovered two mechanisms that may reconcile the differences between the studies using one particular fluorescent sensor, roGFP1-iL, and the earlier studies based on biochemical approaches: (1) an intermediate excitation fluorescence spectrum associated with the roGFP1-iL dimer and (2) a glutathione-mediated shift of the oxidized roGFP1-iL monomer to the dimer form. These two mechanisms likely accounted for the ability of eroGFP1-iL to detect both oxidizing and reducing changes. Formation of the glutathione-mediated stable roGFP1-iL dimer effectively increased the ambient reduction potential at which the sensor has the highest dynamic response in fluorescence intensity change (Figure 8A,B). Using the midpoint potential of roGFP1-iL determined in a dithiol-based redox buffer that did not facilitate dimer formation would underestimate the ER reduction potential.

Measuring the ER Redox State Using Fluorescent Sensors. A family of ratiometric fluorescent sensors based on roGFP1 had been developed in which an insertion made disulfide bond formation between the redox-active cysteine residues more unfavorable, resulting in increased reduction potentials.[34] The member with the highest midpoint potential at −229 mV,[34] roGFP1-iL, has been targeted to the ER of the yeast *P. pastoris*[31] and the human sarcoma cell line HT1080.[33] These studies showed that roGFP1-iL is capable of reporting both oxidizing and reducing changes in the ER, a phenomenon we have replicated in 3T3-L1 fibroblasts in this study (Figures 2−4). This suggests the sensitivity of eroGFP1-iL to both oxidizing and reducing changes reflects ER redox conditions common to many eukaryotic cell lines. However, it is unclear how this reporter is able to detect oxidizing changes in the ER. At the previously published ER redox potential of −150 to −205 mV,[26−28] virtually all of the roGFP1-iL molecules should already be in the oxidized state, thereby reaching a limit on the dynamic range of the redox probe. It is possible that the ER redox potential in *Pichia*, calculated to be approximately −230 mV, is much more reducing than that previously determined for mammalian cells, as Delic et al. had suggested,[31] but that could not account for the observation that roGFP1-iL was able to detect both oxidizing and reducing changes in the ER of mammalian HT1080[33] and CHO[32] cells. The estimate of approximately −230 mV for the ER reduction potential derived by Delic et al. relies on the midpoint potential value of −229 mV for roGFP1-iL determined in a dithiol-based redox buffer.[34] As shown in Figure 8B, the formation of roGFP1-iL dimers in monothiol-based redox buffer effectively increased the reduction potential in which the sensor's fluorescence intensity is dynamically responsive. As a result, the ER reduction potential assessed using eroGFP1-iL is likely higher than −230 mV.

Existence of Redox-Sensitive eroGFP1-iL Dimers and Their Fluorescence Property. We have uncovered two

dx.doi.org/10.1021/bi400052u | *Biochemistry* 2013, 52, 3332−3345

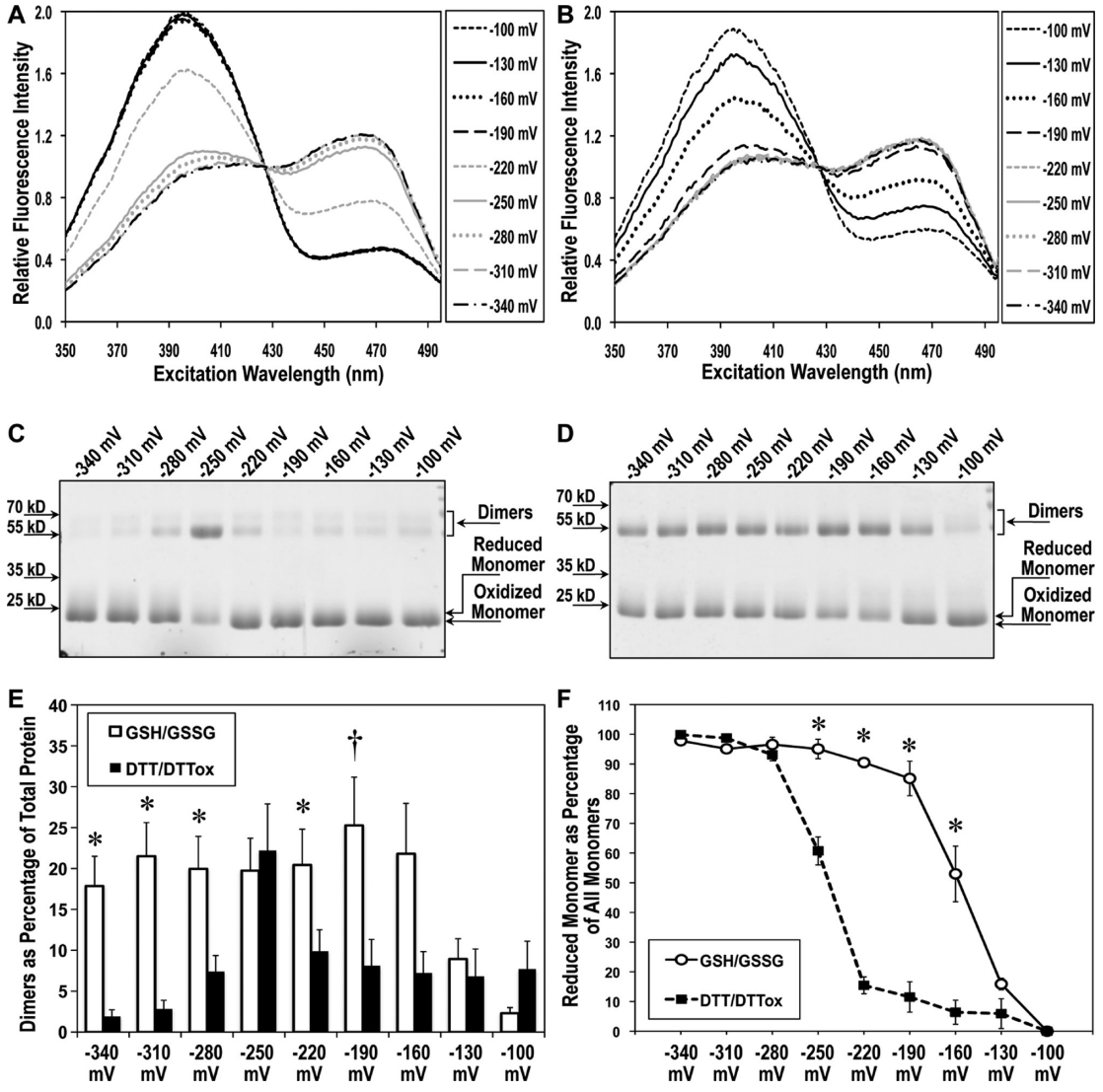

Figure 8. Altered redox states and excitation fluorescence spectra of roGFP1-iL in glutathione- vs DTT-based redox buffer. Excitation fluorescence spectra of purified roGFP1-iL protein at 7.5 μM were obtained after incubation in (A) 2.5 mM oxidized and reduced DTT (DTT/DTTox) or (B) 2.5 mM oxidized and reduced glutathione (GSH/GSSG) maintained at −340, −310, −280, −250, −220, −190, −160, −130, and −100 mV. The redox states of roGFP1-iL after incubation in (C) DTT/DTTox and (D) GSH/GSSG redox buffers were determined using nonreducing SDS−PAGE and visualized with Coomassie stain. The extent of dimerization is expressed in panel E as a percentage of the total protein in nonreducing SDS−PAGE that were dimers in GSH/GSSG (white bars) and DTT/DTTox (black bars) buffers. The tendency of roGFP1-iL to adopt oxidized or reduced monomeric states is depicted in panel F as percentages of monomers in nonreducing SDS−PAGE that were reduced in GSH/GSSG (○) vs DTT/DTTox (●) buffer. Densitometry of Coomassie-stained nonreducing gels was performed using ImageJ. For results in panels E and F, the values were averaged from four independent experiments. Asterisks and daggers denote $p < 0.05$ and $p < 0.06$, respectively, in a paired, two-tailed, Student's t test between samples in GSH/GSSG and DTT/DTTox buffers kept at the same reduction potential.

mechanisms that may explain the ability of eroGFP1-iL to detect oxidizing as well as reducing changes in the ER, and both involve redox-sensitive dimers of eroGFP1-iL. In panels D and E of Figure 4, we showed the presence of a major eroGFP1-iL species with a molecular weight consistent with it being a dimer of eroGFP1-iL. This species could be collapsed by inclusion of a thiol reducing agent in sample loading buffer, suggesting it is a dimer linked by one or more disulfide bridges. This species was also reported previously by van Lith et al.[33] Although neither van Lith et al. nor we offered formal proof by way of purifying the dimerlike species to show it is indeed a dimer of eroGFP1-iL, we demonstrated in Figure 5A that the roGFP1-iL dimer could exist *in vitro* in a redox-dependent fashion. Two lines of evidence supported the idea that the dimer is held together by disulfide bridges involving the redox-sensitive cysteine residues whose redox states dictate the differential excitation fluorescence property of oxidized and reduced roGFP1-iL monomers. First, molecular modeling based on existing GFP dimers demonstrated that a dimer of roGFP1-iL with disulfide bridges between the same cysteine residues (para conformation, C147−C147 and C204−C204) or the opposite cysteine residues (cross conformation, C147−C204) on adjacent monomers is energetically favorable (Figure 5C−F and Figure S2 of the Supporting Information). Second, substitution of the surface alanine residue at position 206 with lysine weakened the tendency of roGFP1-iL to form dimers (Figure 6C,D). This residue is in the proximity of one of the redox-sensitive cysteine residues at position 204 and is also part of a large nearby hydrophobic patch (Figure 6A,B). Decreased levels of A206K

dx.doi.org/10.1021/bi400052u | *Biochemistry* 2013, 52, 3332−3345

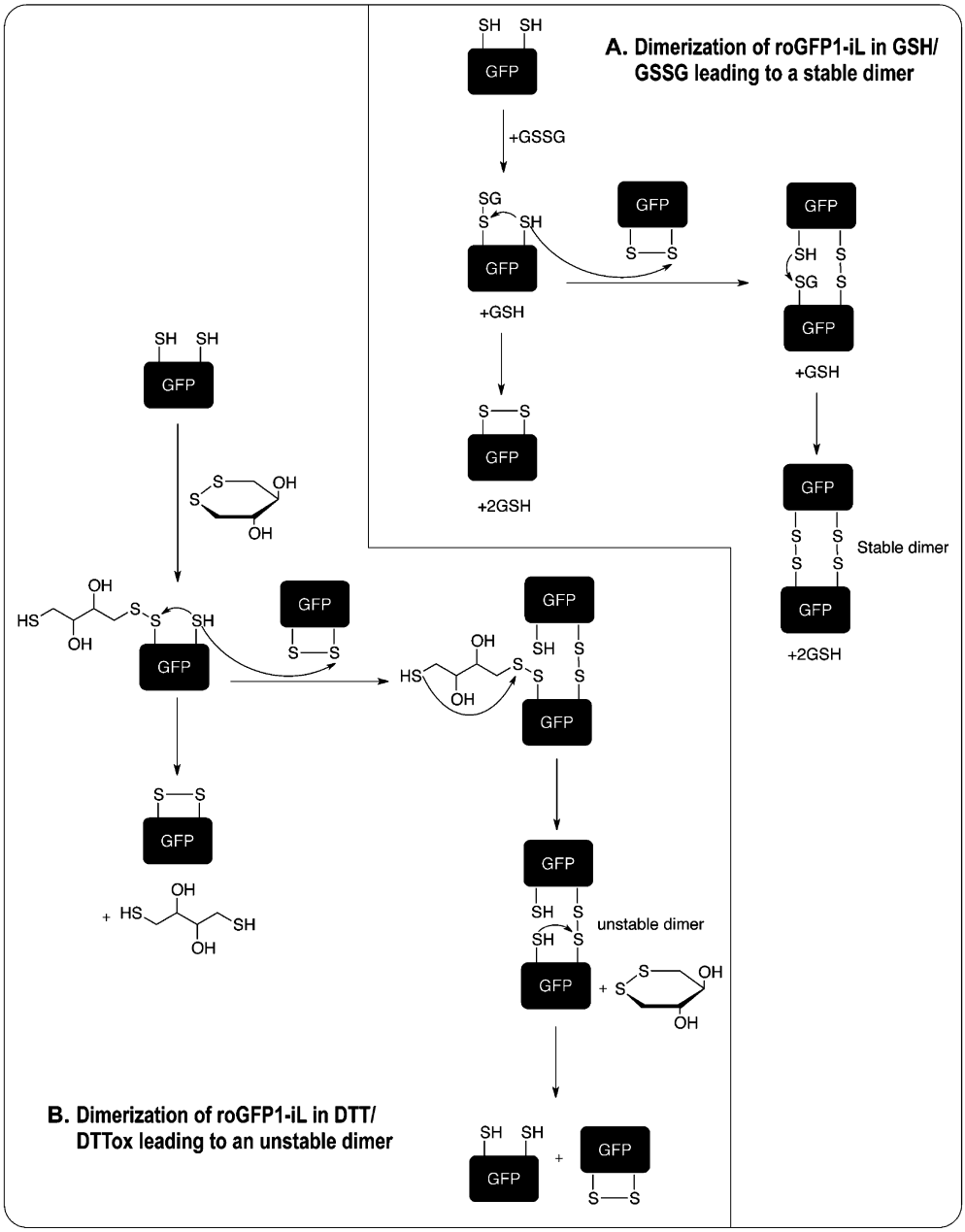

Figure 9. Schematic for roGFP1-iL dimerization pathways in (A) glutathione-based and (B) DTT-based redox buffers.

roGFP1-iL dimers suggest C204 mediates covalent dimer formation.

The excitation fluorescence spectrum of the roGFP1-iL dimer, which resembles a mixture of oxidized and reduced monomers (Figure 7), is one mechanism that allowed eroGFP1-iL to detect oxidizing changes in the ER. At steady state, a majority of eroGFP1-iL existed in dimeric form (Figure 4D), making it possible for a higher oxidized/reduced (380 nm/455 nm) fluorescence ratio to exist upon treatment of cells with oxidizing agents. Conformational differences between oxidized and reduced roGFP1-iL leading to differential ionization of the tyrosine residue in the chromophore are responsible for the ratiometric nature of the sensor.[34] The C147 and C204 residues in a dimer of roGFP1-iL are not expected to adopt the same conformation as an oxidized monomer with a disulfide bridge between the two residues or a reduced monomer in which the residues are farther apart. Most likely, the residues exist in an intermediate conformation in the dimer that leads to a chromophore tyrosine pK_a value between those of oxidized and reduced monomers.

Formation of the Glutathione-Mediated roGFP1-iL Dimer and the Effect on the Reduction Potential. The more important mechanism underlying the ability of eroGFP1-iL to detect oxidizing changes in ER is the increase in the apparent reduction potential of the monomer following glutathione-mediated formation of the dimer. In addition to an abundance of dimer, there were significantly more reduced eroGFP1-iL monomers than there were oxidized monomers in 3T3-L1 fibroblasts under untreated control conditions (Figure 4D). This distribution pattern of eroGFP1-iL proteins *in vivo* resembles that of roGFP1-iL incubated in GSH/GSSG redox buffer at a −160 mV reduction potential *in vitro* (Figure 8D,F). Such a mixture of reduced and oxidized monomers and dimers was also observed in DTT/DTTox redox buffer, but only at a

dx.doi.org/10.1021/bi400052u | *Biochemistry* 2013, 52, 3332−3345

−250 mV reduction potential (Figure 8C,F). The illustration in Figure 9A depicts the process by which glutathione-mediated dimerization of roGFP1-iL changes the distribution of monomers leading to a decreased amount of oxidized monomers relative to reduced monomers. As the redox potential of the environment increases with a higher concentration of GSSG, a reduced roGFP1-iL monomer first becomes glutathionylated, yielding one GSH. At this point, the glutathionylated roGFP1-iL could become an oxidized monomer as the remaining free thiol undergoes intramolecular disulfide bonding to resolve glutathionylation, yielding two GSH molecules overall. Alternatively, the remaining free thiol in glutathionylated roGFP1-iL could undergo intermolecular disulfide bonding with an oxidized roGFP1-iL monomer. This then leads to a mixed disulfide roGFP1-iL dimer with one intermolecular disulfide bridge, one free thiol, and one glutathionylated adduct. Subsequent nucleophilic attack by the free thiol (after deprotonation) will form a second intermolecular disulfide bridge, yielding a stable dimer along with two GSH molecules. Oxidation of a reduced roGFP1-iL by GSSG along both of these two possible routes ultimately results in the transfer of two electrons from two thiols to one GSSG to form a disulfide and two GSH molecules. The difference is that an oxidized roGFP1-iL is trapped in the process of forming a stable dimer, effectively shifting the equilibrium away from oxidized monomers.

In contrast to GSSG, using oxidized DTT as an electron acceptor to oxidize reduced roGFP1-iL will less likely result in the formation of a stable dimer. As illustrated in Figure 9B, a mixed disulfide dimer of roGFP1-iL with a DTT adduct will likely result in an unstable dimer with one disulfide bridge and two free thiols as the second thiol group in DTT mounts a nucleophilic attack to regenerate an oxidized DTT. Unlike in GSH/GSSG, the presence of a roGFP1-iL dimer species in DTT/DTTox at −250 mV had no impact on the midpoint reduction potential of the monomer (Figure 9F).

The schematic in Figure 9A illustrates the formation of a stable roGFP1-iL dimer requiring both a reduced monomer and an oxidized monomer. This is supported by the observation that at an extremely oxidizing state of −100 mV, the amount of dimers was significantly decreased compared to that at lower reduction potentials in GSH/GSSG redox buffer (Figure 8D). Additional support could also be found in panels A and B of Figure 5 in which roGFP1-iL dimer formation was optimal at the lowest diamide concentration tested (0.5 mM). At higher diamide concentrations, dimer formation was hampered. These results underscore the need for both oxidized and reduced monomers to form dimers and provide experimental validation for the model of dimer formation illustrated in Figure 9.

Dynamics of Dimer−Monomer Conversion. Under steady-state conditions, there is likely a rapid equilibrium between dimers and monomers. This possibility is suggested by the difficulty in obtaining large amounts of dimers from the monomers via gel filtration chromatography (Figure 7). This observation stands in stark contrast with the high levels of roGFP1-iL dimers in nonreducing SDS−PAGE (Figures 4D, 5A, 6C, and 8D) under a variety of conditions. However, samples in nonreducing SDS−PAGE had been denatured and treated with NEM to alkylate available thiols, while those in the gel filtration column had not been exposed to NEM and were separated under native conditions in which dimer−monomer exchange could take place.

Factors Complicating the Assessment of the ER Reduction Potential Using eroGFP1-iL. It is probable that the concentration of glutathione in ER will affect the behavior of the sensor in two ways. First, the glutathione concentration will likely affect the rate by which dimers form. Given the rapid equilibrium between roGFP1-iL dimers and monomers and the impact of dimer formation on the levels of oxidized monomers, uncertainty in the rate of dimer formation will make an accurate assessment of the ER redox state difficult to achieve. Second, the proportion of total eroGFP1-iL that is glutathionylated in the ER will have a major impact on the assessment of the ER redox state. Even though glutathionylated eroGFP1-iL differs from reduced eroGFP1-iL in its redox state, we expect these two species to have similar excitation fluorescence spectra because they should have similar degrees of conformational freedom near the redox center. As a result, the uncertainty in the percentage of eroGFP1-iL that is glutathionylated represents another difficulty in assessing ER reduction potential in absolute terms.

Potential Role of Glutathione in Adiponectin Multimerization in the ER. The importance of glutathione in disulfide bond formation in the ER is well-known.[17,19] While glutathione was shown to promote roGFP1-iL dimerization in this study, it is unknown if glutathione facilitates disulfide-mediated protein multimerization in general. One protein whose multimerization status could be affected by glutathione is adiponectin, an adipocyte-secreted hormone that homo-oligomerizes into trimers and disulfide-stabilized 6mers and 18mers.[36] Glutathione enhanced oligomerization of adiponectin 18mers *in vitro*,[37,50] and inhibition of glutathione synthesis by buthionine sulfoximine led to decreased levels of adiponectin in rats. In addition, oligomerization and secretion of adiponectin were enhanced by DsbA-L, an ER-localized adiponectin-interacting protein[51] that was initially characterized as class kappa glutathione *S*-transferase (GSTK1).[52] Even though it contains a thioredoxin-like domain and diverges significantly from canonical GSTs at the sequence level,[51,52] the structural elements for GSH recognition are conserved.[53] Analogous to eroGFP1-iL whose redox-active cysteines can form intramolecular or intermolecular disulfide bonds, adiponectin trimers can form intertrimer or intratrimer disulfide bridges that favor or inhibit, respectively, the assembly of 18mer adiponectin.[37,38]

Epifluorescence Microscopy versus Flow Cytometry in Measuring the ER Redox State. In this study, both flow cytometry and epifluorescence microscopy were used to measure redox changes in the ER of 3T3-L1-eroGFP1-iL cells. Each technique has unique advantages and drawbacks. Flow cytometers are rarely equipped with lasers capable of exciting eroGFP1-iL in the range (around 460 nm) that produces the highest fluorescence when the molecule is in its reduced state. Moreover, the magnitudes of changes in flow cytometry-based 405 nm/488 nm fluorescence intensity ratios in response to diamide and DTT (Figure 4A; 0.27 ± 0.06 and −0.40 ± 0.01, respectively) were smaller than the epifluorescence microscopy-based 380 nm/455 nm intensity ratios (Figures 2A and 3A; 0.79 ± 0.04 and −0.72 ± 0.1, respectively). This suggests the responsiveness of eroGFP1-iL to redox disturbance in 3T3-L1 fibroblasts was lower when eroGFP1-iL was excited with only one wavelength capable of generating varying emission fluorescence depending on the redox state of the molecule. As a result, epifluorescence microscopy, with the ready availability of a wide range of

excitation bandpass filters, and high sensitivity may be better at detecting small ER redox changes than a flow cytometer in which only a 405 or 407 nm laser is available in addition to the ubiquitous 488 nm laser. Nevertheless, flow cytometry may be more desirable in certain applications because of its ability to monitor large numbers of cells quickly and its versatility in measuring additional parameters like cell size or complexity simultaneously.

In summary, this study provides an in-depth analysis of the behavior of the fluorescence-based ER redox-state reporter eroGFP-iL *ex vivo* and *in vitro*. The results showed the reduction potential of roGFP1-iL was dramatically different in glutathione- and DTT-based redox buffers because of glutathione-facilitated dimerization of roGFP1-iL. While it is difficult to determine the absolute ER reduction potential using roGFP1-iL because of the difficulties discussed above, the range of reduction potential in which roGFP1-iL is highly responsive (approximately between −190 and −130 mV) agrees with estimates of ER reduction potential derived from the redox-sensitive glycosylated peptide[26] or the measurement of microsomal GSH/GSSG concentrations.[27] However, the response of the reporter has a reasonable dynamic range, and the use of ratiometric analysis allows for analysis of dynamic redox changes within the ER in real time. Obviously, conclusions regarding the ER redox state drawn from the use of fluorescent reporters must be validated by ensuring the sensor does not behave differently *in vivo* and *in vitro*.

■ ASSOCIATED CONTENT

Supporting Information

QuickTime movies of fluorescence intensity changes of eroGFP-iL after treatment with diamide or DTT for 15 min (Figure S1) and five homology models of roGFP1-iL dimers successfully produced using MODELLER (Figure S2). This material is available free of charge via the Internet at http://pubs.acs.org.

■ AUTHOR INFORMATION

Corresponding Author

*Department of Chemistry and Biochemistry, University of Arizona, MRB Diabetes Research, P.O. Box 245218, Tucson, AZ 85724. E-mail: tsushuen@email.arizona.edu. Telephone: (520) 626-9755. Fax: (520) 626-3644.

Funding

This work is supported by grants from the American Diabetes Association (1-08-JF-54) and the Diabetes Alternative Research and Healthcare Foundation to T.-S.T. S.K.E. and J.A.M. were supported by a grant from the Howard Hughes Medical Institute (52003749) to the University of Arizona Undergraduate Biology Research Program. N.L.H. was supported by the Friends of the Sciences (FOTS) fellowship program at Emory and Henry College.

Notes

The authors declare no competing financial interest.

■ ACKNOWLEDGMENTS

We thank Dr. Jim Remington for providing the roGFP1-iL construct. Confocal images were collected by Brooke Beam in the W. M. Keck Center for Surface and Interface Imaging at the University of Arizona. Flow cytometry analysis was conducted at the Arizona Cancer Center/Arizona Research Laboratories-Division of Biotechnology Cytometry Core Facility (CCSG-CA 023074). Lastly, we thank Kristen L. Sanders for expert graphics support.

■ REFERENCES

(1) Betz, S. F. (1993) Disulfide bonds and the stability of globular proteins. *Protein Sci. 2*, 1551−1558.

(2) Wedemeyer, W. J., Welker, E., Narayan, M., and Scheraga, H. A. (2000) Disulfide bonds and protein folding. *Biochemistry 39*, 7032.

(3) Ruoppolo, M., Vinci, F., Klink, T. A., Raines, R. T., and Marino, G. (2000) Contribution of individual disulfide bonds to the oxidative folding of ribonuclease A. *Biochemistry 39*, 12033−12042.

(4) Braakman, I., Helenius, J., and Helenius, A. (1992) Manipulating disulfide bond formation and protein folding in the endoplasmic reticulum. *EMBO J. 11*, 1717−1722.

(5) Richards, J. E., Scott, K. M., and Sieving, P. A. (1995) Disruption of conserved rhodopsin disulfide bond by Cys187Tyr mutation causes early and severe autosomal dominant retinitis pigmentosa. *Ophthalmology 102*, 669−677.

(6) Tarnow, P., Schoneberg, T., Krude, H., Gruters, A., and Biebermann, H. (2003) Mutationally induced disulfide bond formation within the third extracellular loop causes melanocortin 4 receptor inactivation in patients with obesity. *J. Biol. Chem. 278*, 48666−48673.

(7) Saarela, J., Laine, M., Oinonen, C., von Schantz, C., Jalanko, A., Rouvinen, J., and Peltonen, L. (2001) Molecular pathogenesis of a disease: Structural consequences of aspartylglucosaminuria mutations. *Hum. Mol. Genet. 10*, 983−995.

(8) Pietrangelo, A. (2004) Hereditary Hemochromatosis: A New Look at an Old Disease. *N. Engl. J. Med. 350*, 2383−2397.

(9) Marquardt, T., Hebert, D. N., and Helenius, A. (1993) Post-translational folding of influenza hemagglutinin in isolated endoplasmic reticulum-derived microsomes. *J. Biol. Chem. 268*, 19618−19625.

(10) Tu, B. P., Ho-Schleyer, S. C., Travers, K. J., and Weissman, J. S. (2000) Biochemical basis of oxidative protein folding in the endoplasmic reticulum. *Science 290*, 1571−1574.

(11) Kodali, V. K., and Thorpe, C. (2010) Oxidative protein folding and the Quiescin-sulfhydryl oxidase family of flavoproteins. *Antioxid. Redox Signaling 13*, 1217−1230.

(12) Wajih, N., Hutson, S. M., and Wallin, R. (2007) Disulfide-dependent protein folding is linked to operation of the vitamin K cycle in the endoplasmic reticulum. A protein disulfide isomerase-VKORC1 redox enzyme complex appears to be responsible for vitamin K1 2,3-epoxide reduction. *J. Biol. Chem. 282*, 2626−2635.

(13) Margittai, E., and Bánhegyi, G. (2010) Oxidative folding in the endoplasmic reticulum: Towards a multiple oxidant hypothesis? *FEBS Lett. 584*, 2995−2998.

(14) Sevier, C. S., and Kaiser, C. A. (2002) Formation and transfer of disulphide bonds in living cells. *Nat. Rev. Mol. Cell Biol. 3*, 836−847.

(15) Csala, M., Margittai, E., and Bánhegyi, G. (2010) Redox control of endoplasmic reticulum function. *Antioxid. Redox Signaling 13*, 77−108.

(16) Jessop, C. E., and Bulleid, N. J. (2004) Glutathione directly reduces an oxidoreductase in the endoplasmic reticulum of mammalian cells. *J. Biol. Chem. 279*, 55341−55347.

(17) Chakravarthi, S., and Bulleid, N. J. (2004) Glutathione is required to regulate the formation of native disulfide bonds within proteins entering the secretory pathway. *J. Biol. Chem. 279*, 39872−39879.

(18) Molteni, S. N., Fassio, A., Ciriolo, M. R., Filomeni, G., Pasqualetto, E., Fagioli, C., and Sitia, R. (2004) Glutathione limits Ero1-dependent oxidation in the endoplasmic reticulum. *J. Biol. Chem. 279*, 32667−32673.

(19) Ruddock, L. W. (2012) Low-molecular-weight oxidants involved in disulfide bond formation. *Antioxid. Redox Signaling 16*, 1129−1138.

(20) Sevier, C. S., Qu, H., Heldman, N., Gross, E., Fass, D., and Kaiser, C. A. (2007) Modulation of cellular disulfide-bond formation and the ER redox environment by feedback regulation of Ero1. *Cell 129*, 333−344.

(21) Appenzeller-Herzog, C., Riemer, J., Christensen, B., Sørensen, E. S., and Ellgaard, L. (2008) A novel disulphide switch mechanism in Ero1α balances ER oxidation in human cells. *EMBO J. 27*, 2977−2987.
(22) Baker, K. M., Chakravarthi, S., Langton, K. P., Sheppard, A. M., Lu, H., and Bulleid, N. J. (2008) Low reduction potential of Ero1α regulatory disulphides ensures tight control of substrate oxidation. *EMBO J. 27*, 2988−2997.
(23) Zito, E., Melo, E. P., Yang, Y., Wahlander, Å., Neubert, T. A., and Ron, D. (2010) Oxidative protein folding by an endoplasmic reticulum-localized peroxiredoxin. *Mol. Cell 40*, 787−797.
(24) Wang, X., Wang, L., Wang, X., Sun, F., and Wang, C. C. (2012) Structural insights into the peroxidase activity and inactivation of human peroxiredoxin 4. *Biochem. J. 441*, 113−118.
(25) Day, A. M., Brown, J. D., Taylor, S. R., Rand, J. D., Morgan, B. A., and Veal, E. A. (2012) Inactivation of a peroxiredoxin by hydrogen peroxide is critical for thioredoxin-mediated repair of oxidized proteins and cell survival. *Mol. Cell 45*, 398−408.
(26) Hwang, C., Sinskey, A. J., and Lodish, H. F. (1992) Oxidized redox state of glutathione in the endoplasmic reticulum. *Science 257*, 1496−1502.
(27) Bass, R., Ruddockaaa, L. W., Klappa, P., and Freedman, R. B. (2004) A major fraction of endoplasmic reticulum-located glutathione is present as mixed disulfides with protein. *J. Biol. Chem. 279*, 5257−5262.
(28) Dixon, B. M., Heath, S. H., Kim, R., Suh, J. H., and Hagen, T. M. (2008) Assessment of endoplasmic reticulum glutathione redox status is confounded by extensive ex vivo oxidation. *Antioxid. Redox Signaling 10*, 963−972.
(29) Merksamer, P. I., Trusina, A., and Papa, F. R. (2008) Real-time redox measurements during endoplasmic reticulum stress reveal interlinked protein folding functions. *Cell 135*, 933−947.
(30) Schwarzer, C., Illek, B., Suh, J. H., Remington, S. J., Fischer, H., and Machen, T. E. (2007) Organelle redox of CF and CFTR-corrected airway epithelia. *Free Radical Biol. Med. 43*, 300−316.
(31) Delic, M., Mattanovich, D., and Gasser, B. (2010) Monitoring intracellular redox conditions in the endoplasmic reticulum of living yeasts. *FEMS Microbiol. Lett. 306*, 61−66.
(32) Kolossov, V. L., Leslie, M. T., Chatterjee, A., Sheehan, B. M., Kenis, P. J., and Gaskins, H. R. (2012) Forster resonance energy transfer-based sensor targeting endoplasmic reticulum reveals highly oxidative environment. *Exp. Biol. Med. (Maywood) 237*, 652−662.
(33) van Lith, M., Tiwari, S., Pediani, J., Milligan, G., and Bulleid, N. J. (2011) Real-time monitoring of redox changes in the mammalian endoplasmic reticulum. *J Cell Sci 124*, 2349−2356.
(34) Lohman, J. R., and Remington, S. J. (2008) Development of a family of redox-sensitive green fluorescent protein indicators for use in relatively oxidizing subcellular environments. *Biochemistry 47*, 8678−8688.
(35) Kolossov, V. L., Spring, B. Q., Clegg, R. M., Henry, J. J., Sokolowski, A., Kenis, P. J., and Gaskins, H. R. (2011) Development of a high-dynamic range, GFP-based FRET probe sensitive to oxidative microenvironments. *Exp Biol Med (Maywood, NJ, U.S.) 236*, 681−691.
(36) Briggs, D. B., Jones, C. M., Mashalidis, E. H., Nuñez, M., Hausrath, A. C., Wysocki, V. H., and Tsao, T. S. (2009) Disulfide-Dependent Self-Assembly of Adiponectin Octadecamers from Trimers and Presence of Stable Octadecameric Adiponectin Lacking Disulfide Bonds in Vitro. *Biochemistry 48*, 12345−12357.
(37) Briggs, D. B., Giron, R. M., Malinowski, P. R., Nunez, M., and Tsao, T. S. (2011) Role of Redox Environment on the Oligomerization of Higher Molecular Weight Adiponectin. *BMC Biochem. 12*, 24.
(38) Briggs, D. B., Giron, R. M., Schnittker, K., Hart, M. V., Park, C. K., Hausrath, A. C., and Tsao, T. S. (2012) Zinc enhances adiponectin oligomerization to octadecamers but decreases the rate of disulfide bond formation. *BioMetals 25*, 469−486.
(39) Tsao, T. S., Lodish, H. F., and Fruebis, J. (2002) ACRP30, a new hormone controlling fat and glucose metabolism. *Eur. J. Pharmacol. 440*, 213−221.
(40) Pelham, H. R. (2000) Using sorting signals to retain proteins in endoplasmic reticulum. *Methods Enzymol. 327*, 279−283.
(41) Naviaux, R. K., Costanzi, E., Haas, M., and Verma, I. M. (1996) The pCL vector system: Rapid production of helper-free, high-titer, recombinant retroviruses. *J. Virol. 70*, 5701−5705.
(42) Tsao, T. S., Murrey, H. E., Hug, C., Lee, D. H., and Lodish, H. F. (2002) Oligomerization state-dependent activation of NF-κB signaling pathway by adipocyte complement-related protein of 30 kDa (Acrp30). *J. Biol. Chem. 277*, 29359−29362.
(43) Laemmli, U. K. (1970) Cleavage of structural proteins during the assembly of the head of bacteriophage T4. *Nature 227*, 680−685.
(44) Luo, S., Wehr, N. B., and Levine, R. L. (2006) Quantitation of protein on gels and blots by infrared fluorescence of Coomassie blue and Fast Green. *Anal. Biochem. 350*, 233−238.
(45) Fiser, A., and Sali, A. (2003) Modeller: Generation and refinement of homology-based protein structure models. *Methods Enzymol. 374*, 461−491.
(46) Pédelacq, J. D., Cabantous, S., Tran, T., Terwilliger, T. C., and Waldo, G. S. (2006) Engineering and characterization of a superfolder green fluorescent protein. *Nat. Biotechnol. 24*, 79−88.
(47) Scherer, P. E., Williams, S., Fogliano, M., Baldini, G., and Lodish, H. F. (1995) A novel serum protein similar to C1q, produced exclusively in adipocytes. *J. Biol. Chem. 270*, 26746−26749.
(48) Phillips, G. N. (1997) Structure and dynamics of green fluorescent protein. *Curr. Opin. Struct. Biol. 7*, 821−827.
(49) Zacharias, D. A., Violin, J. D., Newton, A. C., and Tsien, R. Y. (2002) Partitioning of lipid-modified monomeric GFPs into membrane microdomains of live cells. *Science 296*, 913−916.
(50) Iwata, C., Wang, X., Uchida, K., Nakanishi, N., and Hattori, Y. (2007) Buthionine sulfoximine causes endothelium dependent hyper-relaxation and hypoadiponectinemia. *Life Sci. 80*, 873−878.
(51) Liu, M., Zhou, L., Xu, A., Lam, K. S., Wetzel, M. D., Xiang, R., Zhang, J., Xin, X., Dong, L. Q., and Liu, F. (2008) A disulfide-bond A oxidoreductase-like protein (DsbA-L) regulates adiponectin multimerization. *Proc. Natl. Acad. Sci. U.S.A. 105*, 18302−18307.
(52) Pemble, S. E., Wardle, A. F., and Taylor, J. B. (1996) Glutathione S-transferase class kappa: Characterization by the cloning of rat mitochondrial GST and identification of a human homologue. *Biochem. J. 319* (Part 3), 749−754.
(53) Ladner, J. E., Parsons, J. F., Rife, C. L., Gilliland, G. L., and Armstrong, R. N. (2004) Parallel evolutionary pathways for glutathione transferases: Structure and mechanism of the mitochondrial class kappa enzyme rGSTK1-1. *Biochemistry 43*, 352−361.